



This is a repository copy of *On the cross-well dynamics of a bi-stable composite plate.*

White Rose Research Online URL for this paper:
<http://eprints.whiterose.ac.uk/81016/>

Version: Submitted Version

Article:

Arrieta, A.F., Neild, S.A. and Wagg, D.J. (Submitted: 2011) On the cross-well dynamics of a bi-stable composite plate. *Journal of Sound & Vibration*, 330. 3424 - 3441. ISSN 0022-460X

<https://doi.org/10.1016/j.jsv.2011.02.006>

Reuse

Unless indicated otherwise, fulltext items are protected by copyright with all rights reserved. The copyright exception in section 29 of the Copyright, Designs and Patents Act 1988 allows the making of a single copy solely for the purpose of non-commercial research or private study within the limits of fair dealing. The publisher or other rights-holder may allow further reproduction and re-use of this version - refer to the White Rose Research Online record for this item. Where records identify the publisher as the copyright holder, users can verify any specific terms of use on the publisher's website.

Takedown

If you consider content in White Rose Research Online to be in breach of UK law, please notify us by emailing eprints@whiterose.ac.uk including the URL of the record and the reason for the withdrawal request.



eprints@whiterose.ac.uk
<https://eprints.whiterose.ac.uk/>

On the cross-well dynamics of a bi-stable composite plate

Andres F. Arrieta*

*System Reliability and Machine Acoustics, Dynamics and Vibrations Group
Technische Universität Darmstadt, LOEWE-Zentrum AdRIA, Darmstadt, 64289
Germany*

Simon A. Neild, David J. Wagg

Department of Mechanical Engineering, University of Bristol, Bristol, U.K, BS8 1TR

Abstract

Multi-stable composites are a novel type of composites capable of adopting multiple statically stable configurations. Due to the multi-stability property this type of composite material has been considered for several applications, particularly for morphing structures. The change of shape between stable states is achieved by a nonlinear mechanism known as snap-through. Most of the research done on these composites has focused on predicting the configuration after manufacture, its static characteristics and static actuation strategies to induce snap-through. However, these structures will operate subject to dynamic loads. Yet, very little work has been carried out to examine the dynamic behaviour of bi-stable composites. This paper focuses on the study of the cross-well dynamics of a bi-stable composite plate. A simple model previously derived for the dynamics confined to a single stable state is

*Corresponding author. Tel.:+4961517058324

Email address: `andres.arrieta@dyn.tu-darmstadt.de` (Andres F. Arrieta)

extended to include cross-well dynamics. The rich dynamics are experimentally investigated, focusing on cross-well oscillations and the key dynamic features of snap-through. Numerical simulations are obtained and compared to the experimental results showing good agreement. In particular, experimentally observed characteristics suggesting chaotic oscillations for cross-well dynamics are captured well by the proposed model. The results herein could be used for implementing control strategies for both configuration morphing and undesired snap-through suppression of bi-stable composites.

Keywords: bi-stable composites, morphing structures, snap-through, chaotic oscillations

1. Introduction

Composite laminates are increasingly employed in a wide variety of engineering applications. The ever growing need for better performance has resulted in innovative solutions such as structures capable of adjusting properties to perform optimally under different operational conditions, known as adaptive structures [1]. Within this context, the concepts of morphing materials and structures have emerged offering enhanced performance and adaptability for several applications [2, 3]. A promising advance in this direction is the development of curved composite laminates exhibiting multiple statically stable shapes [4]. The multiple configurations arise from asymmetric residual thermal stresses induced during the curing process due to an unsymmetric stacking sequence [5]. The transition between the multiple statically stable states is achieved by a snap-through mechanism which is strongly nonlinear in nature [6]. The multi-stability property has led to these composites

being considered for morphing aerospace structures, since energy is only required to shift between stable shapes [7]. Recently, techniques to produce a wide range of desired stable configurations by designing the induced thermal stresses have been developed [8]. In addition, conceptual morphing applications taking advantage of these capabilities have been proposed [9, 10].

Most of the studies on multi-stable composites have focused on plates exhibiting two stable configurations, known as bi-stable composite plates. Several papers presenting models predicting the shape after the manufacturing process and static characteristics of these composites have been presented [11, 12]. More specifically, these have focused on the identification of the stiffness characteristics [13, 14] and the static load triggering snap-through for bi-stable composites [15, 16, 17]. However, these laminate structures will inevitably be exposed to high levels of dynamic excitation particularly for morphing applications operating on an aeroelastic environment. Early failure could be induced to the structures incorporating multi-stable composites by high levels of vibration. Moreover, undesired snap-through (sudden jumps between stable states) could be triggered by dynamic perturbations. Yet, very little work on the dynamics of multi-stable composites has been carried out to date. The nonlinear response confined to a single stable shape of a bi-stable plate has been experimentally studied [18]. Based on these observations a simple model capturing the complex nonlinear dynamics associated with subharmonic resonances was developed showing very good agreement with experimental results. However, cross-well dynamics were beyond the scope of this work.

A study on the theoretical dynamics of snap-through based on an approx-

imation of the strain field was presented and validated using finite element analysis [19]. Oscillations occurring after a snap-through induced by a quasi-static load were studied showing good qualitative agreement. Simple one degree-of-freedom models describing the dynamics of square bi-stable plates have been presented [20, 21]. Good qualitative agreement was achieved and evidence of complex dynamics for oscillations involving snap-through was shown. Although relevant, these were only preliminary studies leaving open many aspects of the dynamics of these structures, for instance the required levels on dynamic forcing to trigger snap-through were not investigated.

The purpose of this paper is to account for cross-well dynamics extending the study for the dynamics of a bi-stable plate presented in Ref. [18]. A $[0_4 - 90_4]_T$ square bi-stable carbon-fibre epoxy plate similar to that used in Ref. [18] is considered. Experimental tests are performed to study the behaviour of the plate for dynamically induced snap-through. The condition to trigger the snap-through phenomenon is modelled and experimentally validated. The relationship between snap-through force and forcing frequency is obtained in order to identify the minimum dynamic force to trigger the jump phenomenon. Strong nonlinear oscillations showing characteristics of chaotic behaviour are observed for constant changes between stable states, this is for constant cross-well oscillations.

The experimental behaviour is modelled by extending the simple model presented in Ref. [18], including piece-wise defined restoring forces in the nonlinear modal equations. Numerical simulations using the proposed model for time series of the transverse displacement are obtained and compared to experimental results showing good agreement. In particular, the model

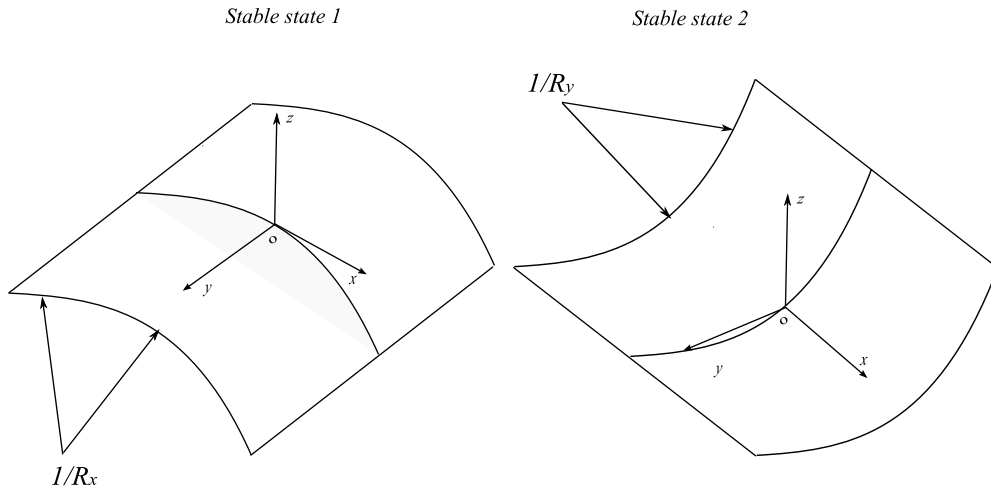


Figure 1: Statically stable states of a bi-stable composite

captures the experimental observations of chaotic behaviour for cross-well dynamics. Diagrams comparing experimentally observed dynamics with numerical simulations are presented for the main parameter range of the bi-stable plate considered herein. Boundaries separating regions in the parameter space marking qualitative changes in the response of the plate are captured accurately by the model. This information, concisely presented in these diagrams, can be potentially used to develop efficient strategies for morphing actuation and stabilization avoiding undesired snap-through of structures incorporating bi-stable composites.

2. Bi-stable composites and snap-through

Bi-stable composites are a type of composites capable of adopting two statically stable shapes. A schematic diagram of the stable configurations of a bi-stable composite plate is shown in Fig. 1. Ideally a bi-stable square plate will exhibit equal curvatures in each of its stable states, this means

that each stable configuration would exhibit equal radii of curvature. The curvature direction for each state is orthogonal to the other as shown in Fig. 1. This property is defined as a perfect orthogonal symmetry between the stable configurations of the plate. As a result of this property, the dynamic response for oscillations confined to a stable state are also orthogonally symmetric, this means that each state will exhibit identical dynamic behaviour only with a rotation of the local frame of $\frac{\pi}{2}$ with respect to the other. However, any real specimen will show imperfections in the final shapes as the manufacturing process has limited accuracy, breaking the perfect symmetry. In particular, the static curvature of each state would have different values for any real specimen. Nevertheless, the response of the stable configurations remains qualitatively symmetric despite manufacturing imperfections.

The change between stable states is achieved via a jump phenomenon known as snap-through [4]. The snap-through mechanism is a sudden event where the structure undergoes large amplitude displacements [22]. This mechanism has been conceptually studied using the schematic model shown in Fig. 2. The underlying principle of the model states that the dynamic response of a system which may undergo a snap-through is only affected by it when a critical displacement is reached triggering the jump phenomenon. Based on this, it is assumed that the oscillations confined to one stable state are unaffected by the presence of the second stable state. Only when a critical displacement is reached the snap-through mechanism plays a part in the dynamics of the bi-stable structure.

This critical displacement is straight forward to define for a lumped mass system such as the one shown in Fig. 2. This is not the case for a contin-

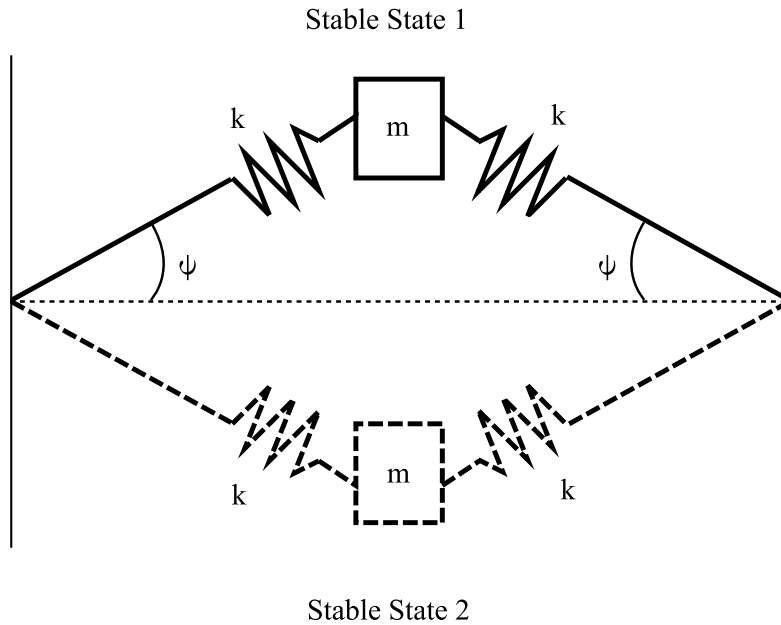


Figure 2: Double-hinge mechanism to model snap-through.

uum such as the bi-stable composites considered here, as each point on the plate undergoes a different displacement when a snap-through is triggered. However, it is assumed that the deflection shape of the bi-stable plate may be modelled with linear mode shapes, such that the relative deflection at any instant of the forcing period between points remains proportional. As a result, once a point reaches its critical displacement a snap-through is triggered as all the points in the plate must have also reached their particular threshold due to the proportionality of mode shapes. This provides a simple condition to define the forcing level required to trigger the snap-through phenomenon. However, the behaviour during the snap-through phenomenon is far more complex and the actual shape of the unstable equilibrium depends on the frequency of excitation triggering the snap-through. Nevertheless, in

a recent paper the saddle shape of the unstable static equilibrium has been shown to be very close to a flat shape. More specifically, the farthest away distance from a flat plane tangent to the bi-stable plate's centre for the stable shapes is one order of magnitude larger in comparison to that of the saddle unstable shape [23]. In view of this to a first approximation, it is assumed that the critical displacement for a point on the plate is given by the static deflection required to reach this flat unstable plane as illustrated in Fig. 3. At this point stable state 2 is defined as the configuration exhibiting a smaller curvature, and stable state 1 having the larger one. The x-direction is chosen to coincide with the curved direction of stable state 1, thus the curved direction of stable state 2 coincides with the y-direction, as can be seen in Fig. 3.

In the ideal case, i.e. for bi-stable plates with perfect orthogonal symmetry, the values for the critical displacement would be equal. However, as mentioned above in reality is difficult to achieve. Furthermore, the more general rectangular shape bi-stable plates are inherently asymmetric due to different static curvatures and length dimensions showing only qualitative symmetry in the response of each configuration. Thus, in general each stable state will exhibit different critical displacement values. For the realistic case, the critical displacement for each stable state is associated with the static deflection of a point lying on a line perpendicular to the flat direction of each configuration. These are defined here using the reference points P_x and P_y , located at (225,150) and (150,225) respectively shown in Fig. 4, where the associated critical displacements for each stable state are presented in Fig. 3. The differences in the static curvature of any real bi-stable plate result in

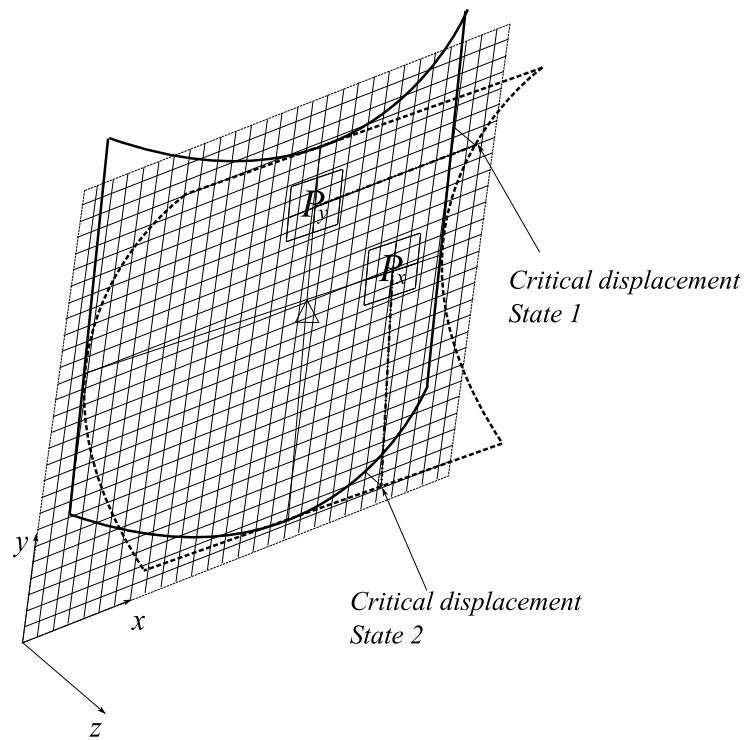


Figure 3: Critical displacements for a bi-stable composite. The flat squared surface approximates the critical deflection shape threshold marking onset of snap-through.

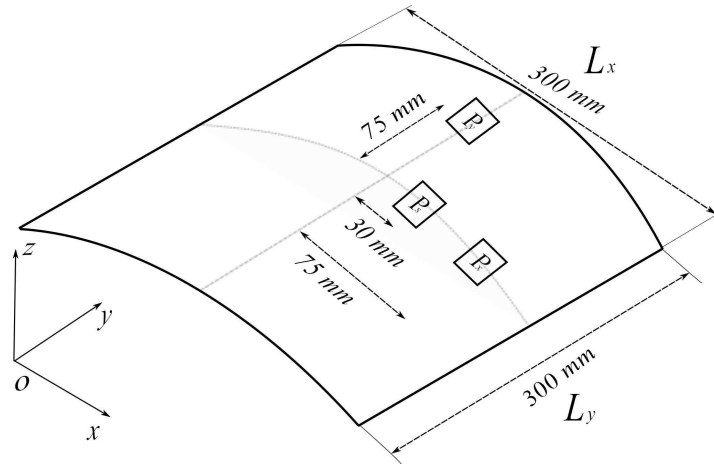


Figure 4: Measured points on the bi-stable plate.

an asymmetric double well potential schematically shown in Fig. 5. It can be seen that the energy required to pass the maximum (hilltop) depends on which state the system is initially oscillating. Hence, the force required to induce snap-through depends on the initial state of the plate, as the critical displacement of one of the states will be smaller than for the other.

3. Cross-well dynamics model

The model for the cross-well dynamics of a bi-stable plate for the studied frequency range is obtained extending that developed for oscillations confined to a single stable configuration (single-well dynamics) presented in Ref. [18]. Here we recall the most relevant results leading to the development of the single-well dynamics model for completeness. Three modes of vibration were observed to characterise the response of the plate around the frequency range where snap-through is most easily triggered. Subharmonic oscillations of order $1/2$ were found to be the dominant nonlinear feature for single-well

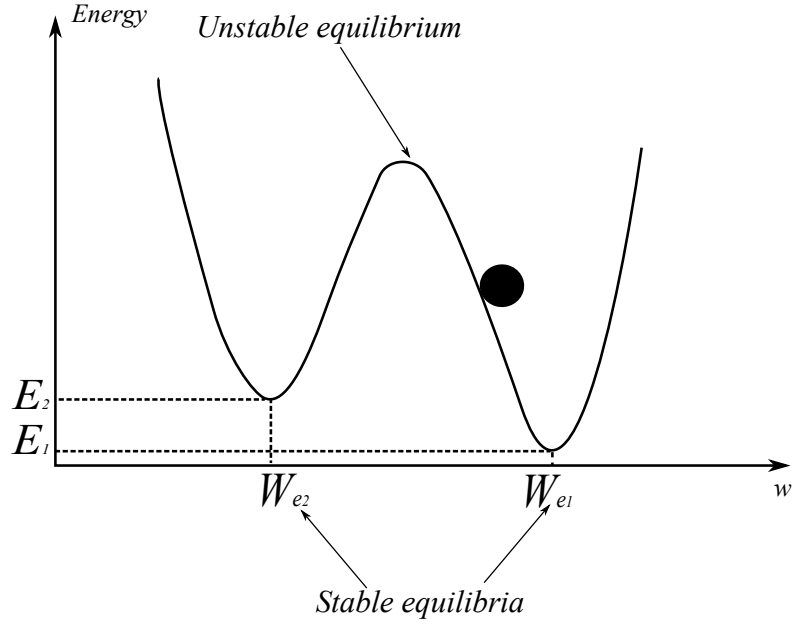


Figure 5: Schematic diagram of a potential well for a bi-stable plate.

dynamics. These oscillations, associated with the dominant effect caused by the static curvature of bi-stable plates, are modelled by including quadratic terms in the time response nonlinear equations. Furthermore, the effects leading to cubic terms in the equations of motion are overshadowed by the dominance of the squared terms generated by the curvature effects. Thus, the cubic terms are neglected as is conventional for curved structures such as shells [24]. The nonlinear modal equations capturing the dynamic features for single-well oscillations were written as [18]

$$\ddot{W}_1 + 2\zeta_{w_1}\omega_{w_1}\dot{W}_1 + \omega_{w_1}^2 W_1 + \alpha_{11}W_1^2 + \alpha_{13}W_1W_3 = \mathcal{Q}_1 \sin(\Omega t), \quad (1)$$

$$\ddot{W}_2 + 2\zeta_{w_2}\omega_{w_2}\dot{W}_2 + \omega_{w_2}^2 W_2 + \alpha_{22}W_2^2 + \alpha_{23}W_2W_3 = \mathcal{Q}_2 \sin(\Omega t), \quad (2)$$

$$\ddot{W}_3 + 2\zeta_{w_3}\omega_{w_3}\dot{W}_3 + \omega_{w_3}^2 W_3 = \mathcal{Q}_3 \sin(\Omega t), \quad (3)$$

where W_1 is the time response coefficient of the transverse displacement for mode w_1 , W_2 is the time response coefficient of the transverse displacement for mode w_2 , W_3 is the time response coefficient of the transverse displacement for mode w_3 , Ω is the forcing frequency, \mathcal{Q}_i is the modal participation factor for mode (i), α_{ij} is the coefficient for the nonlinear quadratic term for an interaction between modes (w_i, w_j). The total transverse displacement, $w(x, y, t)$, for an arbitrary point is given by adding the contribution of each mode to the deflection as

$$w(x, y, t) = \Theta_{w_1}(x, y)_{P_i} W_1(t) + \Theta_{w_2}(x, y)_{P_i} W_2(t) + \Theta_{w_3}(x, y)_{P_i} W_3(t), \quad (4)$$

where $\Theta_{w_1}(x, y)_{P_i}$, $\Theta_{w_2}(x, y)_{P_i}$ and $\Theta_{w_3}(x, y)_{P_i}$ are the values of the mode shapes associated with modes w_1 , w_2 and w_3 evaluated at point P_i .

In order for the model to account for cross-well dynamics, the discussion given in section 2 is employed. As previously stated, only after reaching a critical deflection threshold the snap-through phenomenon would be triggered. This threshold needs to be incorporated in the set of modal equations to account for the bi-stability of the plate. Thus, using the critical displacement condition to mark the onset of snap-through, we introduce piece-wise defined restoring forces into Equations (1)-(3) to obtain,

$$\ddot{W}_{10} + 2\zeta_{w_1^{si}}\omega_{w_1^{si}}\dot{W}_1 + F_1(w) = \mathcal{Q}_1 \sin(\Omega t), \quad (5)$$

$$\ddot{W}_{01} + 2\zeta_{w_2^{si}}\omega_{w_2^{si}}\dot{W}_2 + F_2(w) = \mathcal{Q}_2 \sin(\Omega t), \quad (6)$$

$$\ddot{W}_{11} + 2\zeta_{w_3^{si}}\omega_{w_3^{si}}\dot{W}_3 + F_3(w) = \mathcal{Q}_3 \sin(\Omega t), \quad (7)$$

where the restoring force for each mode is given by

$$F_1(w) = \begin{cases} \omega_{w_1^{s2}}^2(W_1 + w_e^{s2}) + \alpha_{11}(W_1 + w_e^{s2})^2 \\ + \alpha_{13}(W_1 + w_e^{s2})(W_3 + w_e^{s2}), & \text{for } w(x, y, t) < 0 \\ 0, & \text{for } w(x, y, t) = 0 \\ \omega_{w_1^{s1}}^2(W_1 - w_e^{s1}) + \alpha_{11}(W_1 - w_e^{s1})^2 \\ + \alpha_{13}(W_1 - w_e^{s1})(W_3 - w_e^{s1}), & \text{for } w(x, y, t) > 0 \end{cases}, \quad (8)$$

$$F_2(w) = \begin{cases} \omega_{w_2^{s2}}^2(W_2 + w_e^{s2}) + \alpha_{11}(W_2 + w_e^{s2})^2 \\ + \alpha_{13}(W_2 + w_e^{s2})(W_3 + w_e^{s2}), & \text{for } w(x, y, t) < 0 \\ 0, & \text{for } w(x, y, t) = 0 \\ \omega_{w_2^{s1}}^2(W_2 - w_e^{s1}) + \alpha_{22}(W_2 - w_e^{s1})^2 \\ + \alpha_{23}(W_2 - w_e^{s1})(W_3 - w_e^{s1}), & \text{for } w(x, y, t) > 0 \end{cases}, \quad (9)$$

$$F_3(w) = \begin{cases} \omega_{w_3^{s2}}^2(W_3 + w_e^{s2}), & \text{for } w(x, y, t) < 0 \\ 0, & \text{for } w(x, y, t) = 0 \\ \omega_{w_3^{s1}}^2(W_3 - w_e^{s1}), & \text{for } w(x, y, t) > 0 \end{cases}, \quad (10)$$

where $\omega_{w_i^{sj}}$ is the natural frequency of the i mode in the j state, for example $\omega_{w_3^{s1}}$ is the natural frequency of mode w_3 for stable state 1, and the time response and nonlinear coupling coefficients, W_{ij} and α_{ij} were defined above. The equilibrium positions for state 1 and state 2, w_e^{s1} and w_e^{s2} respectively,

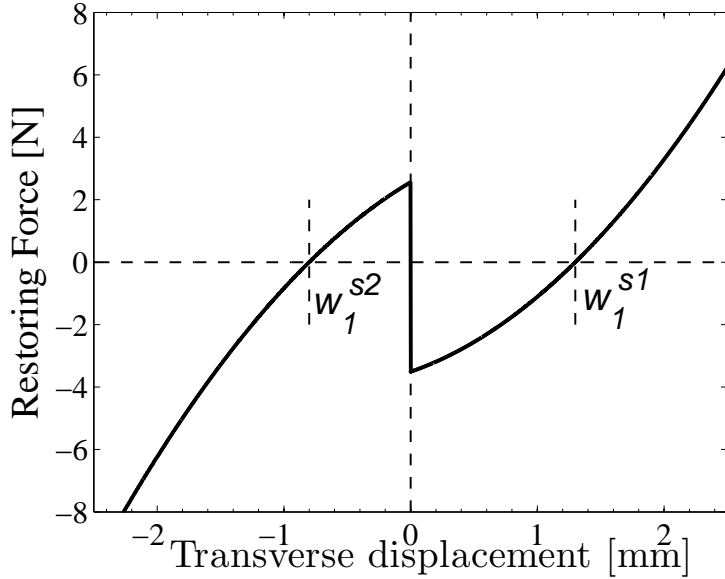


Figure 6: Quadratic restoring force including snap-through nonlinearity for mode w_1 .

are assumed to be equal to the static critical displacements for state 1 and state 2 respectively. The above definition gives a piece-wise quadratic restoring force for modes w_1 and w_2 , and a piece-wise linear restoring force for mode w_3 . For illustration, the restoring force for mode w_1 is schematically shown in Fig. 6. For each mode the defined restoring force gives a double well potential, exhibiting two stable equilibria separated by an unstable equilibrium matching that shown in Fig. 5. By including piece-wise defined restoring forces with a critical displacement condition the model is extended to capture oscillations between stable configuration (cross-well dynamics). Hence, a model for single-well and cross-well oscillations is obtained. These two types of dynamic behaviour encompass the whole range of responses shown by the bi-stable plate around the frequency range of interest.



Figure 7: Bi-stable plate mounted on a shaker used as external excitation source. (a) Stable state 1. (b) Stable state 2. (Reproduced with the kind permission of the Journal of Intelligent Material Systems and Structures [25])

4. Experimental dynamic response

In this section, the procedure to experimentally study the dynamic response in the parameter range of interest for the bi-stable plate is presented. The main objective of the experimental tests is to investigate the key dynamic features of cross-well oscillations and the role of snap-through in the response.

4.1. Experimental assembly

A bi-stable plate with unsymmetric stacking sequence $[0_4 - 90_4]_T$ and dimension 300 by 300 mm similar to that used in Ref. [18] is employed as test specimen for this study. The two stable configurations of the specimen are shown in Figs. 7(a) and 7(b). The experimental specimen is attached to an electromechanical shaker used as external source of vibration. The external forcing is applied at the mounting point coinciding with the centre of the bi-

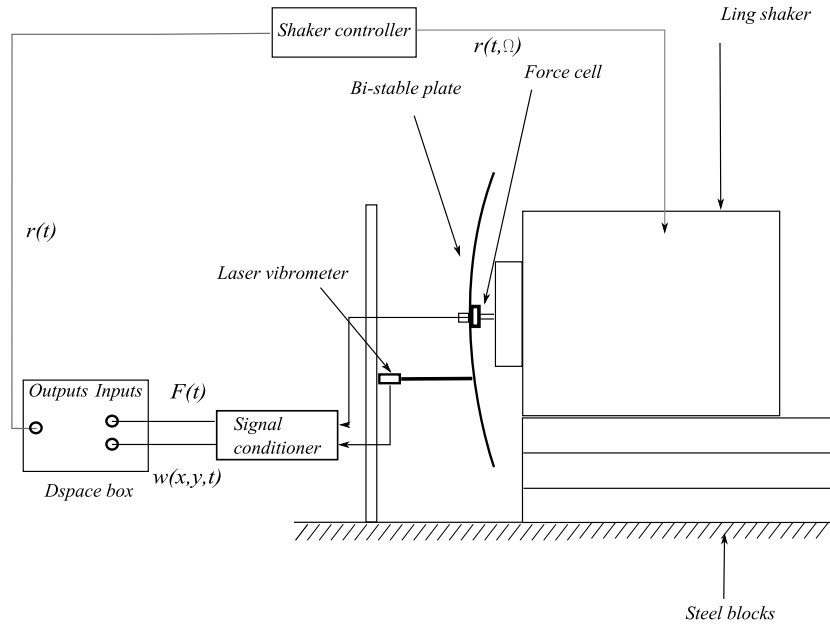


Figure 8: Schematic diagram of the experimental rig.

stable plate to simulate free edge boundary conditions. A load cell is located between the shaker and the plate to measure the external force acting on the specimen. The experimental specimen is mounted on a steel table of large mass in order to avoid interaction between the plate and its surroundings. A differential laser vibrometer is used to measure relative displacement between the centre of the specimen and a given point on the plate in order to obtain time series for the displacement response. The signals from the vibrometer and the load cell are filtered and amplified using a signal conditioner. These signals are then read using an analog-to-digital acquisition box and the data is stored using a digital interface. A controller monitoring the amplitude of the force sensed by the load cell is implemented to minimise the impact of the shaker dynamics in the experiments. A schematic diagram of the

experimental assembly is shown in Fig. 8 where labels can be found for all the mentioned equipment. The experimental assembly used to perform the experiments is shown in Fig. 9 and the material properties of the bi-stable plate are listed in Table 1.

<i>Property</i>	<i>Fibrevol.</i>	<i>Ply thickness</i>	<i>Density ρ</i>	E_{xx}	E_{yy}	G_{xy}^a	$\nu_{xy}^a = \nu_{yx}^a$
	[%]	[mm]	[kg/m ³]	[GPa]	[GPa]	[GPa]	
<i>Value</i>	57.7	0.131	1570	164	12	4.6	0.3

Table 1: Material properties for a ply of HexPly 8557 IM7 used to manufacture the bi-stable plate experimental specimen.

4.2. Dynamic response confined to a stable state

The most relevant dynamic features of the response for each stable state are recalled in this section, for details on the experimental study refer to Ref. [18].

The nonlinear behaviour of the bi-stable plate is studied using *Experimental Frequency Response Diagrams*, which can be thought of as combining the concepts of Frequency Response Functions (FRF) and Poincaré maps to provide information of modal properties and nonlinear oscillations as described in Ref. [18]. These diagrams are obtained using a single harmonic (of constant amplitude) force input for stepped frequency sweeps. Peak-to-peak amplitudes of response are sampled over several consecutive forcing periods of steady state motions and plotted using the forcing frequency as parameter. For a linear response, a single amplitude value is sampled for consecutive periods for a given forcing frequency. Conversely, several points for a given

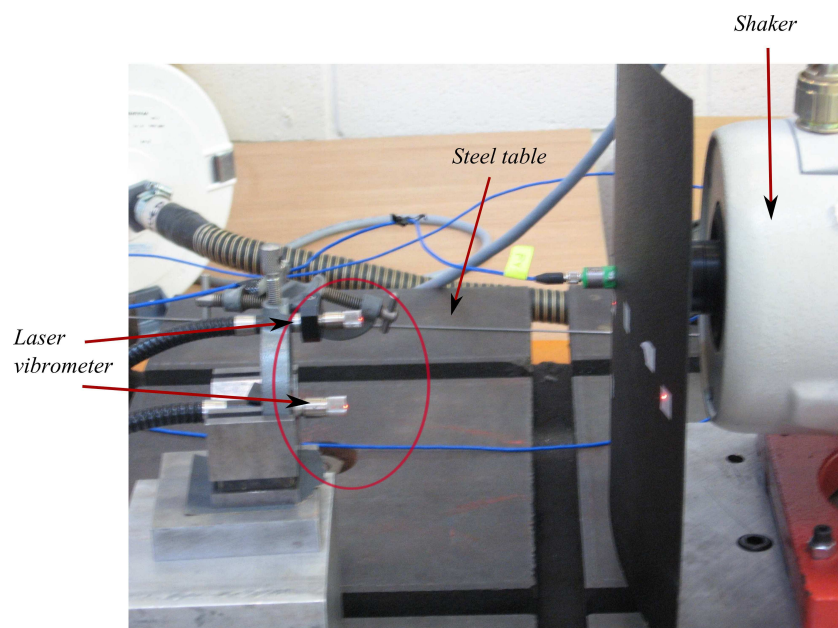


Figure 9: Experimental Assembly. Ling shaker V405, vibrometer OFV-552. (Reproduced with the kind permission of Nonlinear Dynamics [18])

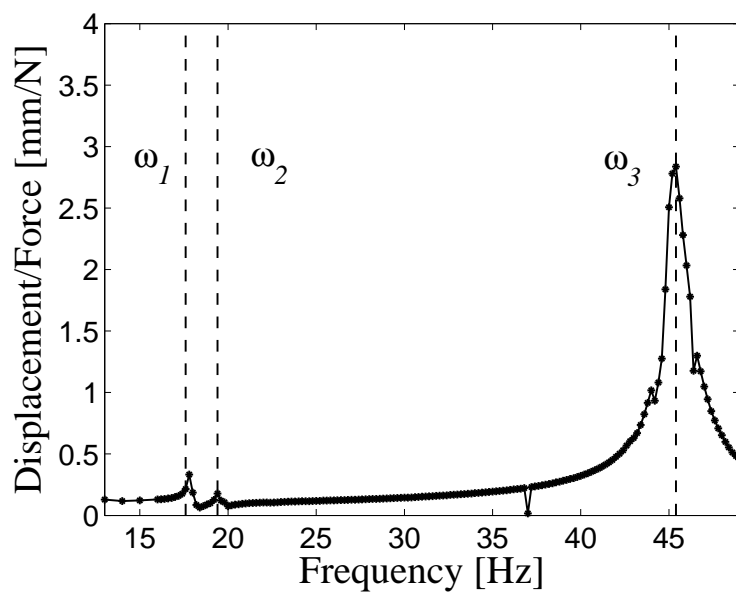


Figure 10: Experimental receptance (Displacement/Force) FRF for point P_x on stable state 1. Forcing amplitude $F_o = 1.0$ N, frequency range $\Omega=[13, 49]$.

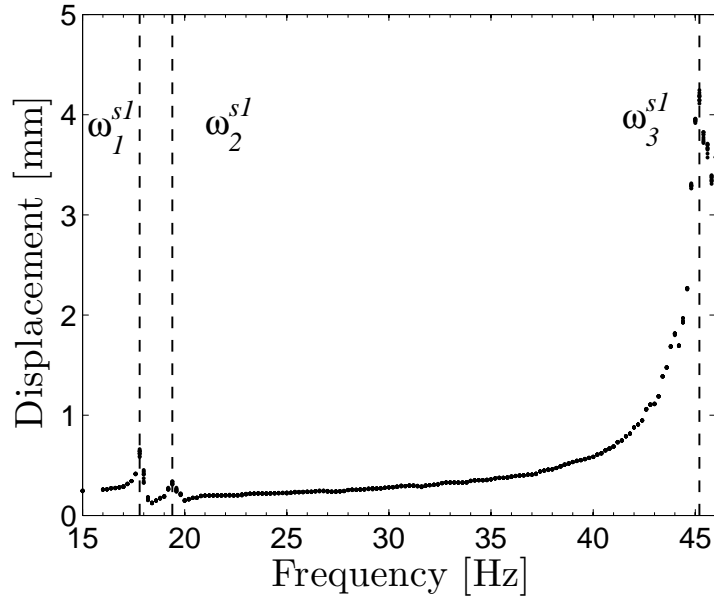


Figure 11: Experimental frequency response diagram for point P_x in stable state 1. $F_o=1.0$ N, frequency range $\Omega=[15, 46]$.

frequency indicate the presence of multiple harmonics in the response signalling nonlinear oscillations. Results obtained for points P_x and P_y shown in Fig. 4 are used to characterise the response of the bi-stable plate. The experimental frequency response diagram of point P_x in stable state 1 obtained for a low forcing amplitude of 1 N is shown in Fig. 11. Three modes dominate the low amplitude response, mode w_1^{s1} at 17.6 Hz, mode w_2^{s1} at 19.4 Hz and mode w_3^{s1} at 45.4 Hz. Figure 12 shows the diagram for a forcing amplitude of 5 N of point P_x for stable state 1. Nonlinear oscillations, signalled by multiple points in the experimental frequency response diagrams [26], can be seen at twice the frequency of modes w_1^{s1} and w_2^{s1} .

The same study is performed here for stable state 2. The low amplitude

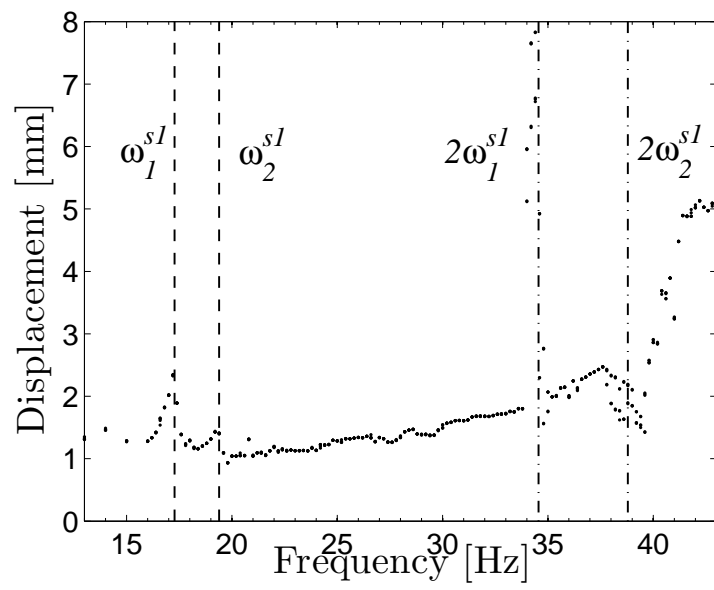


Figure 12: Experimental frequency response diagram for point P_x in stable state 1. $F_o=5.0$ N, frequency range $\Omega=[13, 43]$.

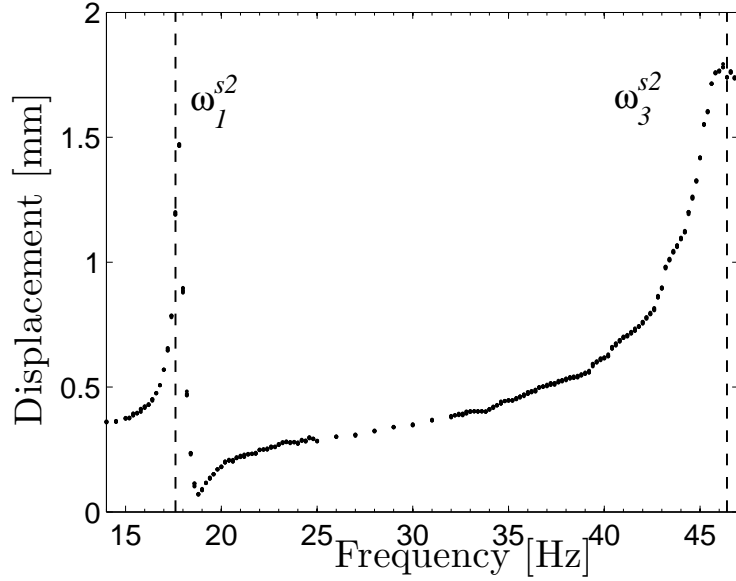


Figure 13: Experimental frequency response diagram for point P_y in stable state 2. $F_o=1.5$ N, frequency range $\Omega=[15, 47]$.

experimental frequency response diagram of point P_y in stable state 2 for a forcing amplitude of 1.5 N is shown in Fig. 13. Modes w_2^{s2} and w_3^{s2} , at 17.8 Hz and 46.2 Hz appear in the response. Note that the response of point P_y in stable state 2 is qualitatively similar to that of point P_x due to the orthogonal symmetry of the response. However as orthogonal symmetry is broken due to manufacturing imperfections, mode w_1^{s2} does not appear in Fig. 13 as for stable state 2 the point P_y lies on a nodal line of this mode. The natural frequency of mode w_1^{s2} is identified to be at 16.9 Hz.

A comparison for the regions showing nonlinear response for point P_x in stable state 1 and point P_y in stable state 2 is given in Fig. 14. When two amplitude points appear for a given forcing frequency, the presence of two

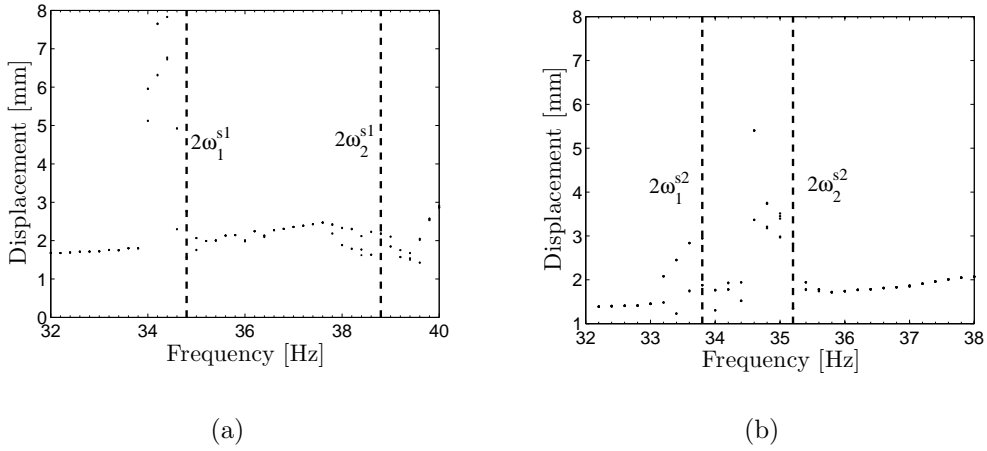


Figure 14: Subharmonic oscillations of modes w_1 and w_2 for a forcing amplitude $F_o = 5$ N, for (a) point P_x in state 1 and (b) point P_y in state 2. Vertical lines show the regions of subharmonic oscillations at twice the frequency of modes w_1 and w_2 in both stable states.

dominant harmonics in the response is signalled. This type of response coincides with $1/2$ subharmonic oscillations of modes w_1 and w_2 for both stable states as shown in Ref. [18], matching well known results in the nonlinear dynamics literature [27, 28]. For both frequency ranges, when comparing the two stable states it can be seen that there is a small shift in the frequencies where subharmonic oscillations for modes w_1 and w_2 occur, however the response is qualitatively similar. The previous results confirm the assumption of a qualitative orthogonally symmetric response for the stable states of the plate, however due to the manufacturing imperfections it is not perfect.

4.3. Critical displacement condition

The critical displacements for points P_x and P_y are statically measured giving 5 mm and 1.5 mm respectively. Thus, the deflection thresholds to change from stable state 2 to stable state 1 is 1.5 mm, and 5 mm from stable

state 1 to stable state 2. The radii of curvature are 0.6 m and 10 m for stable state 1 and 2 respectively. These values represent static characteristics of the plate, therefore we perform dynamic measurements of the critical displacement to reveal any dynamic effects not captured by the critical displacement condition. For practical reasons the deflection of point P_s located at (180,150), which is closer to the centre of the plate on the same perpendicular line as point P_x , is measured. This is done as deflections underwent by point P_s are smaller in comparison to those of point P_x , ensuring that the large displacements can be measured with the available laser vibrometer. The defined deflection threshold would remain valid due to the proportionality of the deflection shape assumed in section 2 for the plate, which implies that when point P_s reaches its critical displacement point P_x must also have done so. The statically measured critical displacement for point P_s is 0.2 mm.

The displacement instants before a snap-through is triggered from stable state 2 to stable state 1 for point P_s as a function of the forcing frequency is presented in Fig. 15. As with the experimental frequency response diagrams (Figs. 11-14), the displacement is measured over consecutive forcing periods with the maximum displacement for each forcing period plotted. Multiple displacement amplitudes are observed for some frequencies due to subharmonic behaviour. However the subharmonic response is small such that the displacements are clustered around a mean value which indicates the critical displacement threshold. It can be seen that away from the linear and subharmonic resonances the dynamic critical displacement matches the static critical displacement value for point P_s . The value of the critical displace-

ment overshoots its static value around resonances as inertial forces dominate the response for these frequencies. Thus, the elastic forces (stiffness) of the plate dominate the snap-through phenomenon when the plate is driven at frequencies away from resonance, whereas inertial effects become dominant around both linear and nonlinear resonances. Therefore, the condition marking the onset of the snap-through phenomenon varies with the frequency of the dynamic excitation. Hence, the threshold incorporating this dynamic effect is redefined as a *dynamic critical displacement* in section 5.

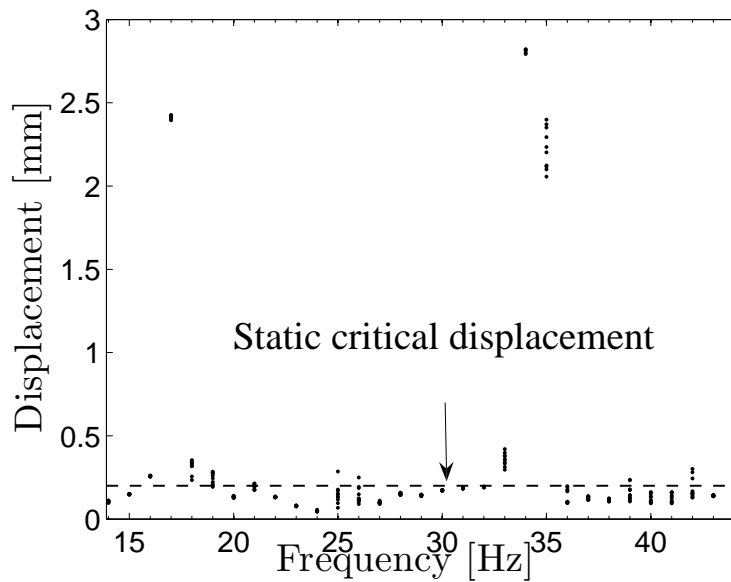


Figure 15: Experimental peak-to-peak displacement for point P_s instants before a dynamically induced snap-through from state 2 to state 1 is triggered. This marks the critical displacements as a functions of the forcing frequency for snap-through from state 2 to state 1.

4.4. Cross-well dynamic response

Having identified a dynamic condition marking the onset of snap-through in section 4.3, the force required to achieve this deflection is also measured. As for the dynamic critical displacement, the force required to induce snap-through from state 2 to state 1 is measured over consecutive forcing periods, the results are shown in Fig. 16. The force vs frequency relationship is in good agreement with previous works on snap-through of shells, see for example [29]. Once more, the results are clustered around a value showing that the forcing level before snap-through remains almost constant. This force threshold marks the boundary separating oscillations confined to stable state 2 with those confined to stable state 1.

Due to the asymmetry of the potential wells of the system, seen in Fig. 5, once a snap-through from the lower energy to the higher energy well is triggered, the system remains oscillating confined to this state. It can be seen that the regions requiring less forcing input to trigger snap-through are around the linear and subharmonic resonances of the bi-stable plate in state 2, at 16.9, 17.8, 34, 36 and 46.2 Hz. This result shows that the characteristics of the dynamic response, both linear and nonlinear, for oscillations confined to a potential well, influence the snap-through dynamics. This fact has not been highlighted in previous dynamic studies considering snap-through in the of bi-stable plates [9, 20, 21].

To illustrate the process of snap-through from state 2 to state 1 the displacement and force response for a forcing frequency of 35 Hz are shown in Fig. 17. Inspecting Figs. 17(a) and 17(c) at around 1.2 s a very noticeable spike appears in both the displacement and force time series, this marks the

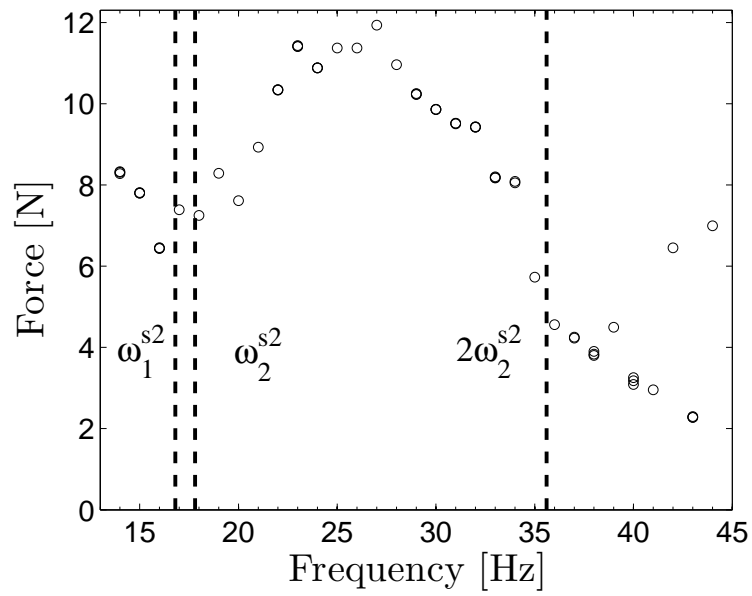


Figure 16: Experimental forcing amplitude required to dynamically induce snap-through from state 2 to state 1. The vertical lines indicate the relationship between the modes and subharmonic oscillations with the regions requiring less actuation input to dynamically triggering snap-through.

instant where the snap-through is dynamically triggered. An interesting observation is the difference between the DC shift of the displacement response before and after the snap-through. This is approximately 0.27 mm which is very close to the static out-of-plane displacement that point P_s undergoes to reach the other stable configuration. The time series then settles down to zero as laser vibrometers cannot measure DC components in the displacements.

As the forcing amplitude is further increased a dynamic snap-through from state 1 to state 2 is induced. Due to the asymmetry in the shapes of the stable configurations, the difference between the energy required to overcome the unstable equilibrium separating the stable equilibria is different. As a result, when a snap-through is induced from an initial condition lying in the potential well of stable state 1, the energy given to the plate is sufficient to trigger a snap-through back from stable state 2 to state 1 as shown in Fig. 18. The first snap-through is induced at around 2.44 s, where a marked change in both the displacement and force time responses is seen. In this limiting case, after this event the plate returns to oscillate around stable state 1 for a brief time followed by a second snap-through at 2.6 s.

If the energy of the input is increased the system immediately jumps back to stable state 1, triggering a continuous steady state snapping between stable configurations (continuous cross-well oscillations) as shown in Fig. 19(a). This response shows a very erratic non-repeating behaviour in the displacement time series. Due to the high levels of energy involved in this type of oscillations the forcing input interacted with the response of the plate as can be seen in Fig. 19(b). The non-repeating character of the displacement response and the observed peaks in the power spectrum presented

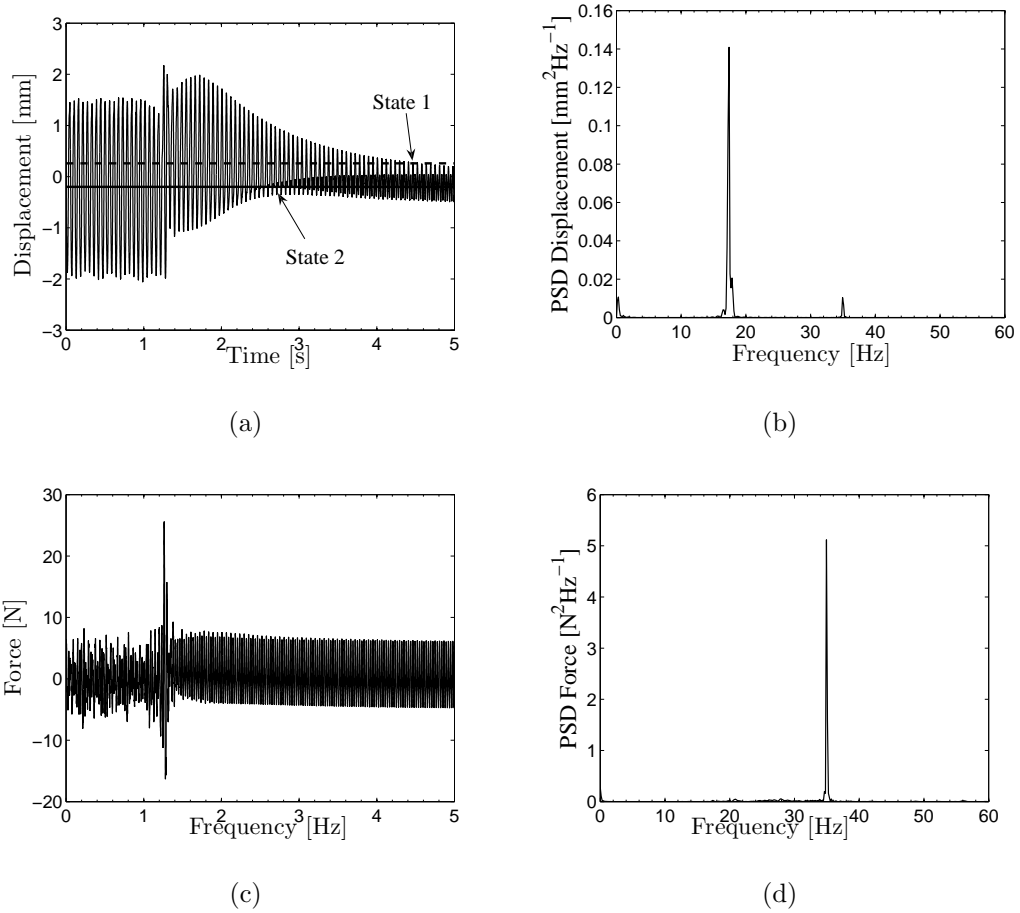
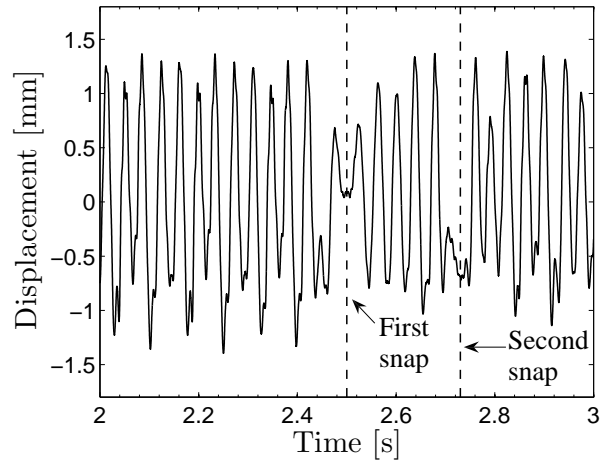
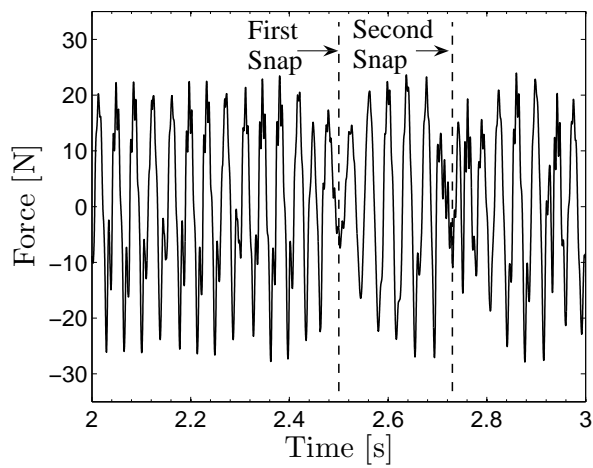


Figure 17: Experimental response for a dynamically induced snap-through from state 2 to state 1. Forcing frequency $\Omega=35.0$ Hz. (a) Displacement time response. (b) Displacement power spectrum. (c) Force time response. (d) Force power spectrum.



(a)



(b)

Figure 18: Experimental response for a dynamically induced snap-through from state 1 to constant snap-through. Forcing frequency $\Omega=27.0$ Hz. (a) Displacement time response. (b) Force time response.

in Fig. 19(c) at incommensurate frequencies of the modes, as well as at the modal frequencies and their integer multiples, are indications of a chaotic response [30]. Inspecting the spectrum with a logarithmic scale for the Power Spectrum Density (PDS) of the displacement in Fig. 21, broadband peaks are observed for the response reaffirming the case for a chaotic behaviour of the plate for this dynamic regime. Figure 20 shows the forcing amplitude required to trigger this behaviour as a function of the forcing frequency. Similarly to Fig. 16, this force threshold marks the boundary separating oscillations confined to stable state 1 with the region of constant snap-through between stable states.

5. Simulation results and model validation

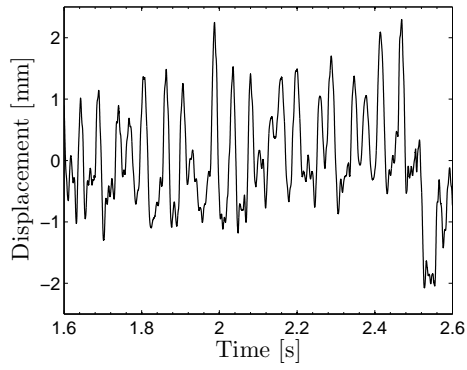
To validate the proposed model, numerical simulations are obtained and compared to the experimental results for the cross-well dynamics of the plate. Initially, we introduce the unmodelled dynamic effect on the threshold marking the onset of the snap-through phenomenon. This is achieved by defining the dynamic critical displacements as

$$w_{\text{crit}}^{s1}(\Omega) = \frac{2}{(\Omega - \omega_{w_1^{s1}})^2 + d_1\Omega} + \frac{2}{(\Omega - 2\omega_{w_1^{s1}})^2 + d_2\Omega} + w_{\text{static}}^{s1}, \quad (11)$$

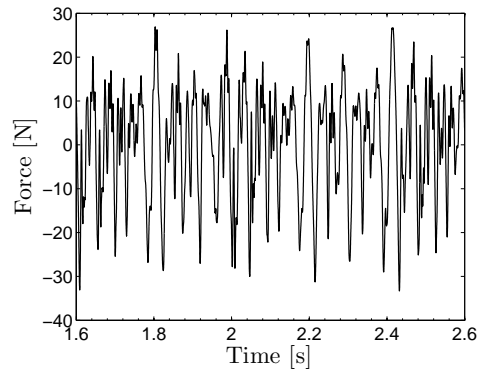
and for state 2 by

$$w_{\text{crit}}^{s2}(\Omega) = \frac{2}{(\Omega - \omega_{w_2^{s2}})^2 + e_1\Omega} + \frac{2}{(\Omega - 2\omega_{w_2^{s2}})^2 + e_2\Omega} + w_{\text{static}}^{s2}, \quad (12)$$

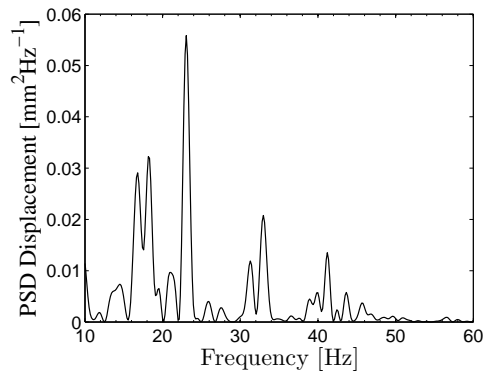
where Ω is the forcing frequency, d_1 , d_2 , e_1 and e_2 are constants related to the amplitude of the critical displacement around the resonances, which are identified from the experiments. The static critical displacements are equal



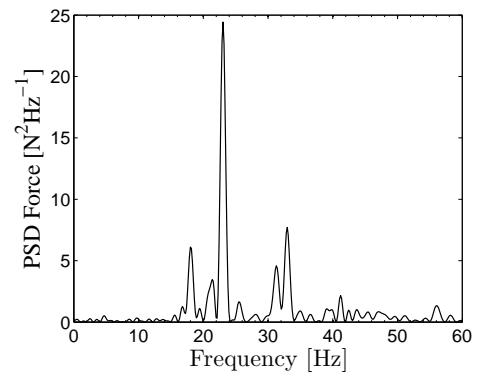
(a)



(b)



(c)



(d)

Figure 19: Experimental response for a constant snap-through between stable states. Forcing frequency $\Omega=23.0$ Hz. (a) Displacement time response. (b) Displacement power spectrum. (c) Force time response. (d) Force power spectrum.

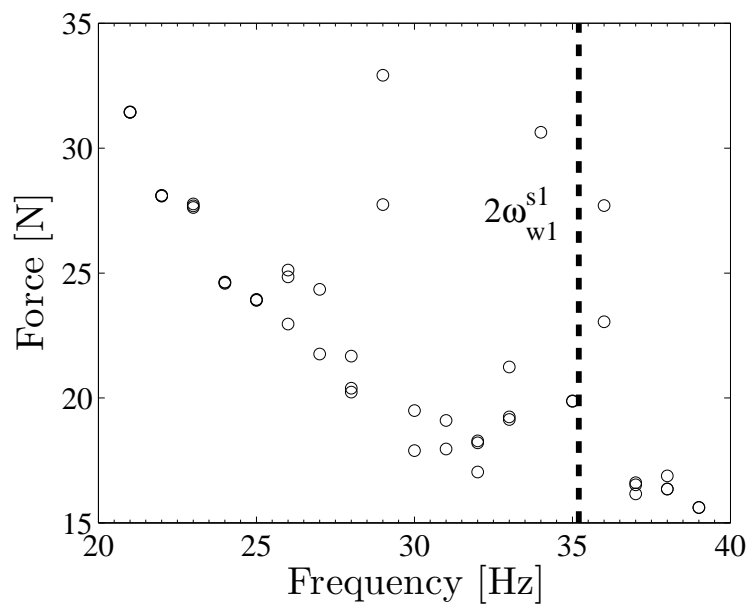


Figure 20: Experimental forcing amplitude required to dynamically induce snap-through from state 1 to constant snap-through oscillations as a functions of the forcing frequency.

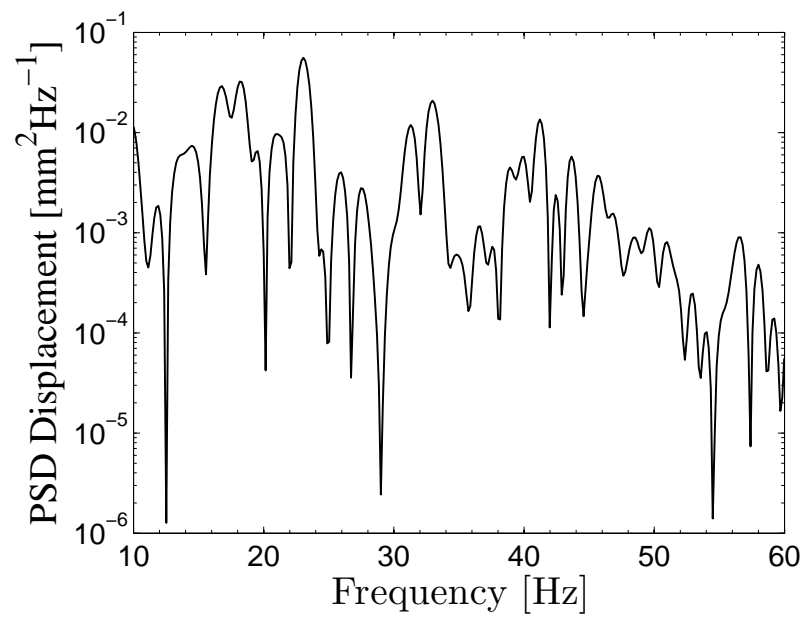


Figure 21: Experimental displacement PSD with logarithmic scale for continuous snap-through between stable states for a forcing frequency of $\Omega=23.0$ Hz. Broadband peaks are observed indicating a chaotic response.

to the equilibrium position for each state, that is for state 1

$$w_{\text{static}}^{s1} = w_e^{s1}, \quad (13)$$

and for state 2,

$$w_{\text{static}}^{s2} = w_e^{s2}, \quad (14)$$

To validate the above definition given in Eqs. (11)-14, Fig. 22 shows the comparison between the simulated dynamic critical displacement to the experimental mean critical displacement calculated by averaging the consecutively sampled values plotted in Fig. 15. Averaging the values for a given forcing frequency does not smooth out the underlying dynamic behaviour and allows for clearer comparison with the simulated results. Good agreement can be seen for the dynamic critical displacement w_{crit}^{s2} marking the onset of snap-through from state 2 to state 1 with the proposed function. A similar condition can be formulated for the snap-through from state 1 to the steady state constant snap-through between stable states. However, due to the chaotic nature of the response of the bi-stable plates before these oscillations, it is impossible to obtain experimentally the critical displacement as a function of the frequency with the available measuring equipment. Nevertheless, it is hypothesized that the mechanism is essentially the same as for the snap-through from state 2 to state 1.

A simulated time series for a snap-through from stable state 2 to stable state 1 is shown in Fig. 23 for a forcing frequency of 39 Hz and a forcing amplitude of 5.5 N. Once the snap-through is triggered the resulting oscillations are restricted to state 1, as not enough energy is given to the system to snap back to state 2 and into constant snap-through. A simulated time series

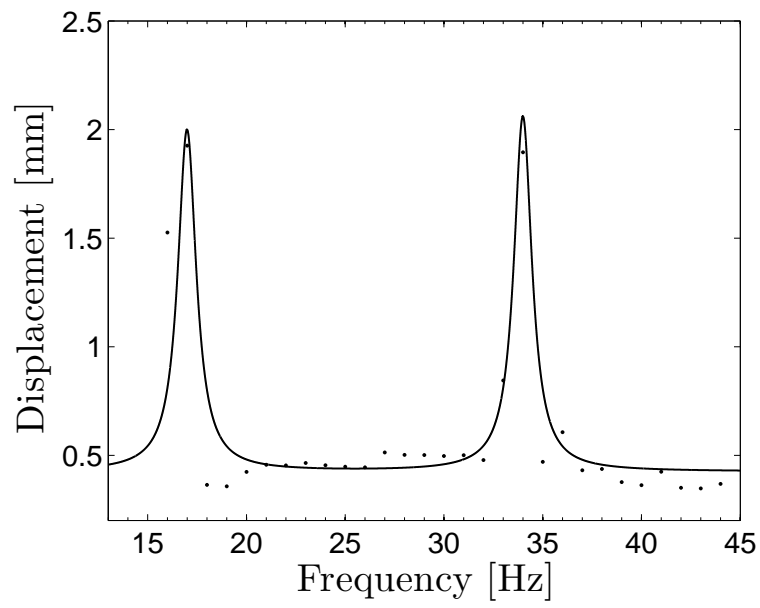


Figure 22: Comparison between experimental (dots) and simulated (solid line) dynamic critical displacement.

showing oscillations involving constant snap-through between stable states is given in Fig. 24(a) for a forcing frequency of 23 Hz. The time response shows a non-repeating behaviour where non-periodic oscillations between the minimum and maximum values appear to occur near a dominant frequency. The power spectrum of the time series shows more than three peaks at incommensurate frequencies, around 7, 13, 41 and 43 Hz in Fig. 24(b), matching the results previously shown in Fig. 19(a). Furthermore, the simulated PSD of the displacement plotted with logarithmic scale shows broadband peaks in Fig. 25. This compares qualitatively with experimental results shown in Fig. 21, matching the observed indications pointing to a chaotic behaviour given in section 4.4.

To show the global validity of the model, the different regions of linear and nonlinear responses using the forcing amplitude and frequency as parameters are compared summarising the different dynamic behaviours exhibited by the bi-stable plate. The comparison of the experimental and simulated dynamic response for oscillations initially starting in state 2 is presented in Fig. 26. Four distinctive regions are observed: linear oscillations confined to stable state 2, subharmonic oscillations of modes w_1^{s2} and w_2^{s2} , linear oscillations confined to stable state 1, and constant snap-through oscillations between stable state 2 and stable state 1. The experimental boundary marking the change from stable state 2 to stable state 1 (solid line with \diamond markers) is compared to the simulated boundary (solid line) showing a good match. It can be seen that the simulated results predict quite accurately the different boundaries marking the onset of the subharmonic oscillations and the jump from state 2 to state 1, except for the range between 19-25 Hz. An

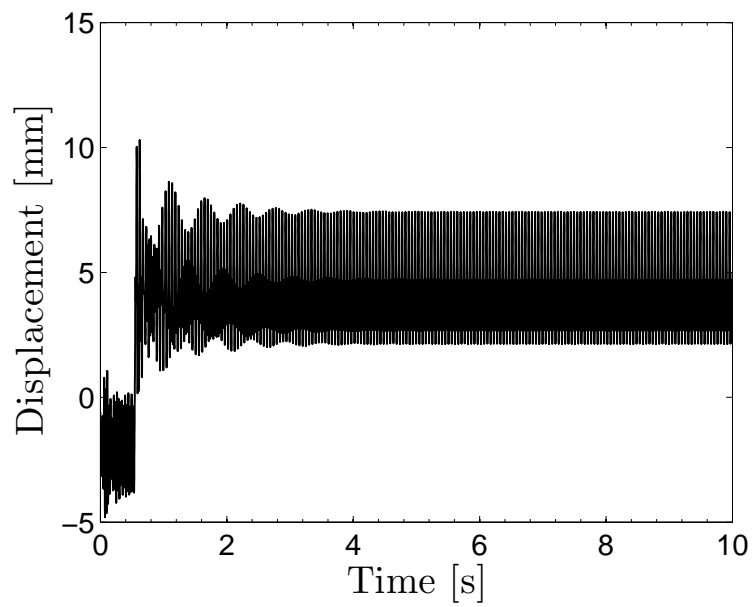


Figure 23: Simulated response for a dynamically induced snap-through from state 2 to state 1. Forcing frequency $\Omega=39.0$ Hz. Forcing amplitude $F_o=15.6$ N. Compare with experimental data in Fig. 17(a).

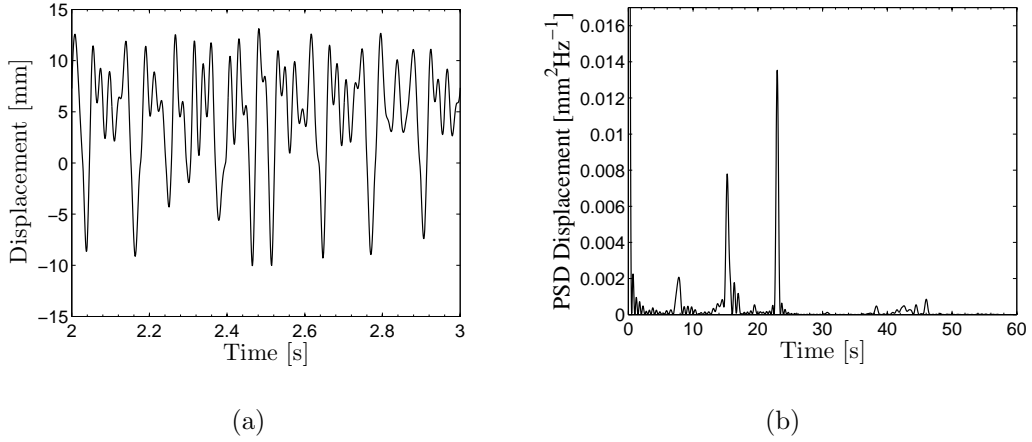


Figure 24: Simulated response for a dynamically induced snap-through from state 1 to constant snap-through. Forcing frequency $\Omega=23.0$ Hz. Forcing amplitude $F_o=47.5$ N. (a) Displacement time response. (b) Displacement power spectrum. Compare with experimental data in Figs. 19(a) and 19(b).

antiresonance lying in this frequency range is over predicted by the model. Thus, the model shows a stiffer behaviour of the plate around this frequency range resulting on a much higher level of forcing required to deflect the plate past its critical displacement. In addition, a good match is achieved between the simulated boundaries marking the onset of the subharmonic oscillations for mode w_1 (dashed line) and mode w_2 of stable state 2 (dotted line) with the experimental results (shown with * and \circ markers respectively). As the force parameter is increased the experimental boundary separating linear oscillations in stable state 1 from constant snap-through oscillations (solid line with \times markers) is reached, this is compared to the simulated results in the following.

Figure 28 shows the comparison of the experimental and simulated dynamic response for oscillations initially starting in state 1. Three distinctive

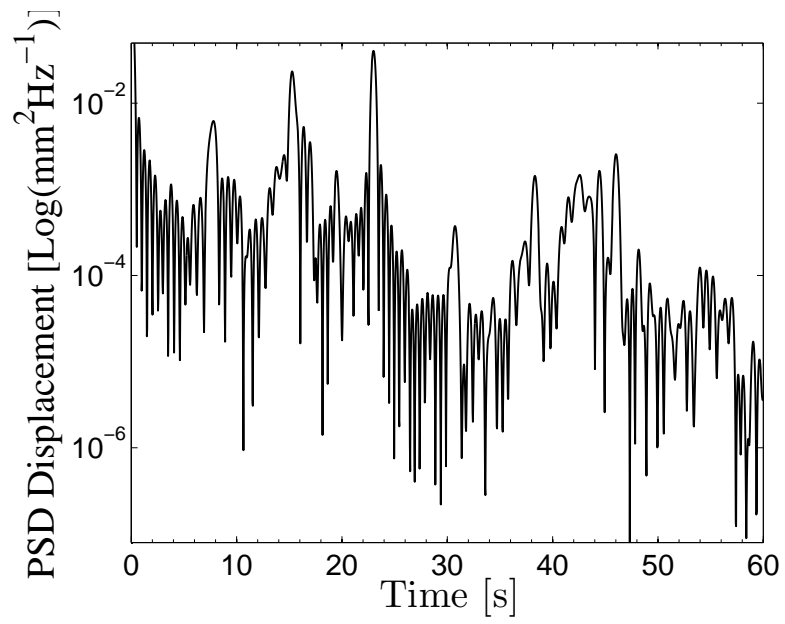


Figure 25: Simulated power spectrum for the displacement response of a dynamically induced snap-through from state 1 to constant snap-through showing broadband peaks. Forcing frequency $\Omega=23.0$ Hz. Forcing amplitude $F_o=47.5$ N. Compare with experimental data in Fig. 21.

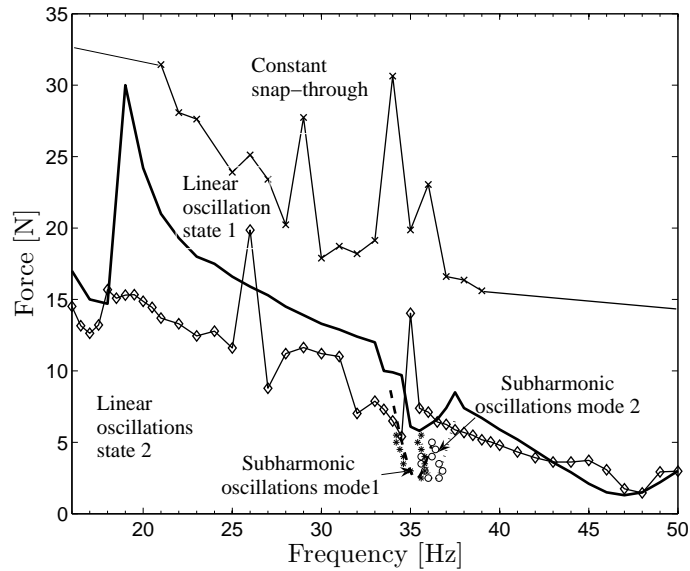


Figure 26: Different dynamic behaviours for oscillations with initial condition in stable state 2. Four distinctive regions are observed: linear oscillations confined to stable state 2, subharmonic oscillations of modes w_1^{s2} and w_2^{s2} , linear oscillations confined to stable state 1, and constant snap-through oscillation between stable state 2 and stable state 1. In addition three experimental and simulated force boundaries separating the regions are shown: force for snap-through from stable state 2 to state 1 (solid line with \diamond markers and solid line respectively), subhamornic oscillations of mode w_1^{s2} (* markers and dashed line respectively), subhamornic oscillations of mode w_2^{s2} (\circ markers and dotted line respectively). The force boundary between oscillations in stable state 1 and constant snap-through is also included (solid line with \times markers), however not compared to simulated results.

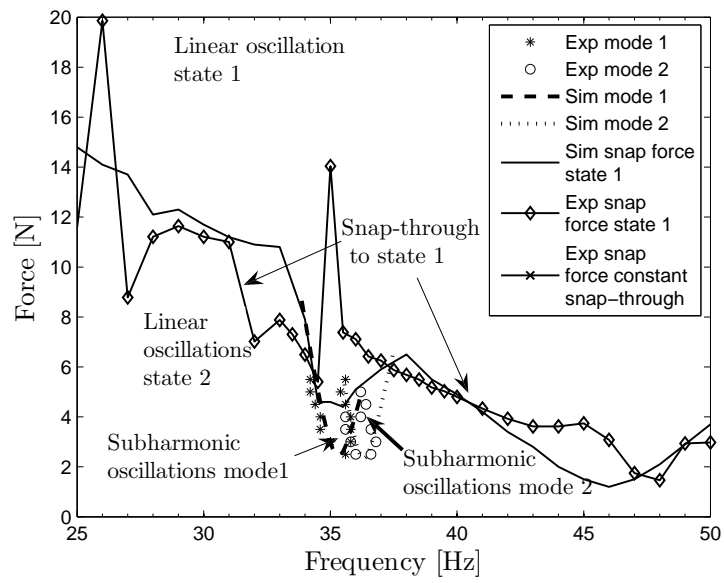


Figure 27: Detail of regions around the subharmonic oscillations showing the dynamic behaviour for oscillations starting on stable state 2.

regions are observed, linear oscillations confined to stable state 1, two regions of subharmonic resonance of modes w_1^{s1} and w_2^{s1} , and constant snap-through oscillation between stable state 1 and stable state 2. In this case, for the experimental (solid line with \times markers) and simulated boundaries (solid line) marking the onset of constant snap-through between stable states only a qualitative match was achieved. This might be a result of the strong interaction between the plate and the shaker for these levels of excitation. However, it still provides an indication of the boundary marking the onset of this dynamic behaviour. As for oscillations starting in state 2, a good match between the experimental (shown as $*$ and \circ markers respectively) and simulated boundary (shown as dashed and dotted lines respectively) marking the onset of subharmonic oscillations for modes w_1^{s1} and w_2^{s1} of stable state 1 is achieved. Figures 26-28 provide a detailed summary of the rich dynamic behaviour exhibited by the studied bi-stable structure. As mentioned in section 2, due to asymmetries in the bi-stable plates distinct levels of forcing arise for triggering snap-through from each stable state. This is particularly advantageous for morphing purposes as perfect orthogonal symmetry introduces difficulties for configuration control, as for any given static or dynamic actuation load both stable equilibria (each one associated to each state) have almost the same likeliness to attract the motion of the plate triggering continuous cross-well oscillations. However, for other applications such as energy harvesting perfect symmetry can be exploited to achieve broadband large amplitude energy conversion [31].

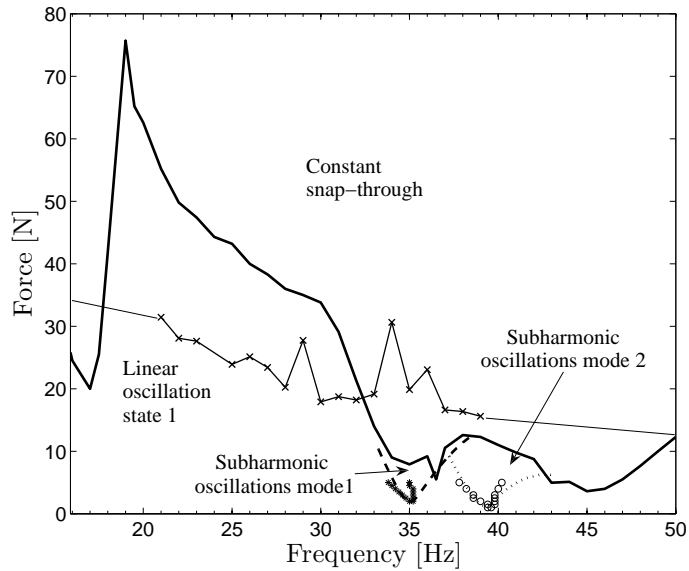


Figure 28: Complete dynamic behaviour for oscillations starting in stable state 1. Three distinctive behaviours are observed, linear oscillations confined to stable state 1, two regions of subharmonic resonance of modes w_1^{s1} and w_2^{s1} , and constant snap-through oscillation between stable state 1 and stable state 2. In addition three experimental and simulated force boundaries separating the regions are shown: force for snap-through from stable state 1 to constant snap-through (solid line with \times markers and solid line respectively), subhamornic oscillations of mode w_1^{s1} ($*$ markers and dashed line respectively), subhamornic oscillations of mode w_2^{s1} (\circ markers and dotted line respectively).

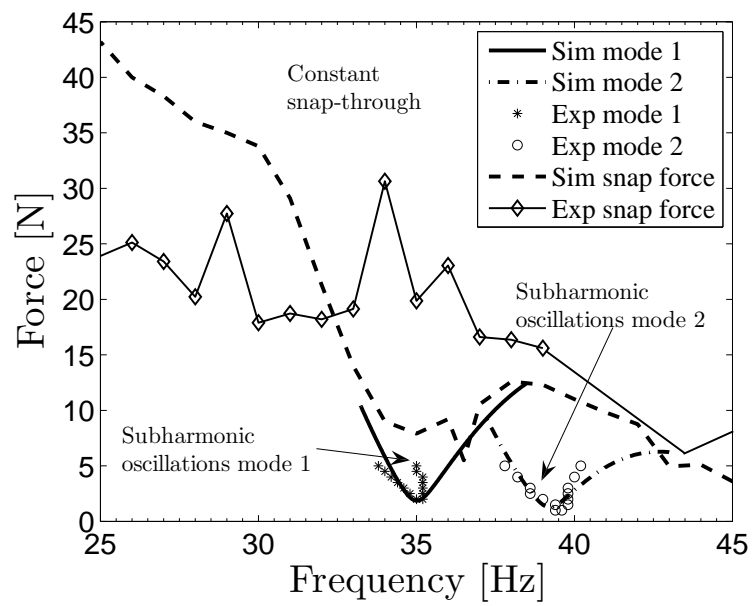


Figure 29: Detail of regions around the subharmonic oscillations showing the dynamic behaviour for oscillations starting on stable state 1.

6. Conclusions

The dynamics for a bi-stable composite plate are experimentally investigated and modelled focusing on oscillations between stable states or cross-well dynamics. It is shown that the experimental condition to trigger a snap-through is governed by a displacement threshold that is frequency dependent, defined as the dynamic critical displacement. Experimental results showed the force required to dynamically trigger snap-through is strongly related to the linear and nonlinear resonances of the plate. This observation shows that features of the dynamic response for oscillations confined to a potential well influence the dynamic response leading to snap-through. This fact has not been highlighted in previous studies on the dynamics of bi-stable plates. Additionally, for oscillations involving snap-through between stable states a complex nonlinear behaviour is observed. In particular, for steady state oscillations between stable states evidence indicating the characteristics of a chaotic response is observed.

A simple model extending the results from Ref. [18] including the critical displacement conditions to account for cross-well dynamics of the bi-stable plate is developed. A good qualitative match for the cross-well dynamics of the bi-stable plate is obtained with the model. The snap-through phenomenon is captured, in particular the snap-through force from stable state 2 to stable state 1 is closely matched. Moreover, the model captured the experimentally observed complex continuous snap-through oscillations from one state to the other, matching the characteristics of a chaotic response. Figures 26-28 summarise the rich dynamic features of the response of the bi-stable plate. This information could be used for selecting efficient con-

trol and actuation strategies both to stabilize a desired state and to achieve morphing configuration for applications implementing bi-stable composites. Furthermore, asymmetries in the response of the bi-stable structures could be designed in other to facilitate morphing and/or impede dynamic perturbations. Concerning the critical displacement condition, more research is needed to shed light onto the actual shape of the unstable equilibrium through which bi-stable composites dynamically. This is necessary for closer approximations of the critical displacement condition.

References

- [1] R. L. Clark, W. R. Saunders, G. P. Gibbs, Adaptive structures: Dynamics & Control, John Wiley & Sons, 1998.
- [2] R. Maute, G. W. Reich, Integrated multidisciplinary topology optimization approach to adaptive wing design, *Journal of Aircraft* 43 (2006) 253–263.
- [3] C. Thill, J. Etches, I. Bond, K. D. Potter, P. M. Weaver, Morphing skins, *Aeronautical Journal* 117 (2008) 117–139.
- [4] M. L. Dano, M. W. Hyer, Thermally-induced deformation behavior of unsymmetric laminates, *International Journal of Solids and Structures* 35 (1998) 2101–2120.
- [5] M. Schlecht, K. Schulte, Advanced calculation of the room-temperature shapes of unsymmetric laminates, *Composite Materials* 33 (1999) 1472–1490.

- [6] S. V. Sokorin, A. V. Terentiev, On modal interaction, stability and nonlinear dynamics of a model two d.o.f. mechanical system performing snap-through motion, *Nonlinear Dynamics* 16 (1998) 239–257.
- [7] M. R. Schultz, M. W. Hyer, Snap-through of unsymmetric cross-ply laminates using piezoceramic actuators, *Journal of Intelligent Material Systems and Structures* 14 (2003) 795–814.
- [8] K. D. Potter, P. M. Weaver, A concept for the generation of out-of-plane distortion from tailored frp laminates, *Composites Part A: Applied Science and Manufacturing* 35 (2004) 1353–1361.
- [9] C. G. Diaconu, P. M. Weaver, F. Mattioni, Concepts for morphing airfoil sections using bi-stable laminated composite structures, *Thin-Walled Structures* 46 (2008) 689–701.
- [10] F. Mattioni, P. M. Weaver, K. D. Potter, M. I. Friswell, The application of residual stress tailoring of snap-through composites for variable sweep wings, in: 47th AIAA/ASME/ASCE/AHS/ASC Structures, Structural Dynamics, and Materials Conference.
- [11] M. L. Dano, M. W. Hyer, Snap-through of unsymmetric fiber-reinforced composite laminates, *International Journal of Solids and Structures* 39 (2002) 175–198.
- [12] W. Hufenbach, M. Gude, L. Kroll, Design of multistable composites for application in adaptive structures, *Composites Science and Technology* 62 (2002) 2201–2207.

- [13] P. Giddings, C. Bowen, R. Butlera, H. Kim, Characterisation of actuation properties of piezoelectric bi-stable carbon-fibre laminates, *Composites Part A: Applied Science and Manufacturing* 39 (2008) 697–703.
- [14] F. Mattioni, P. M. Weaver, K. D. Potter, M. I. Friswell, Analysis of thermally induced multistable composites, *International Journal of Solids and Structures* 45 (2008) 657–675.
- [15] M. L. Dano, M. W. Hyer, Sma-induced snap-through of unsymmetric fiber-reinforced composite laminates, *International Journal of Solids and Structures* 40 (2003) 5949–5972.
- [16] K. D. Potter, P. M. Weaver, A. A. Seman, S. Shah, Phenomena in the bifurcation of unsymmetric composite plates, *Composites Part A: Applied Science and Manufacturing* 38 (2007) 100–106.
- [17] M. R. Schultz, M. W. Hyer, R. B. Williams, W. K. Wilkie, D. J. Inman, Snap-through of unsymmetric laminates using piezocomposite actuators, *Composites Science and Technology* 66 (2006) 2442–2448.
- [18] A. F. Arrieta, S. Neild, D. Wagg, Nonlinear dynamic response and modelling of a bi-stable composite plate for applications to adaptive structures, *Nonlinear Dynamics* 58 (2009) 259–272.
- [19] C. G. Diaconu, P. M. Weaver, A. F. Arrieta, Dynamic analysis of bi-stable composite plates, *Journal of Sound and Vibration* 22 (2009) 987–1004.
- [20] A. F. Arrieta, F. Mattioni, S. A. Neild, P. M. Weaver, D. J. Wagg, K. D. Potter, Nonlinear dynamics of a bi-stable composite laminate plate with

applications to adaptive structures, in: 2nd European Conference for Aero-Space Sciences.

- [21] A. Carrella, F. Mattioni, A. A. Diaz, M. I. Friswell, D. J. Wagg, P. M. Weaver, Static and dynamic analysis of a bistable plate for application in morphing structures, in: 7th European conference on structural dynamics, July 7-9, Southampton, UK.
- [22] J. M. T. Thompson, *Instabilities and Catastrophes in Science and Engineering*, John Wiley & Sons, 1982.
- [23] A. Pirrera, D. Avitabile, P. M. Weaver, Bistable plates for morphing structures: A refined analytical approach with high-order polynomials, *International Journal of Solids and Structures* 47 (2010) 3412–3425.
- [24] O. Thomas, C. Touzé, E. . Luminais, Non-linear vibrations of free-edge thin spherical shells: Experiments on a 1:1:2 internal resonance, *Nonlinear Dynamics* 49 (2007) 259–284.
- [25] A. F. Arrieta, D. J. Wagg, S. A. Neild, Dynamic snap-through for morphing of bi-stable composite plates, *Journal of Intelligent Material Systems and Structures* published online 21 December 2010. DOI: 10.1177/1045389X10390248 (2010).
- [26] A. F. Arrieta, *Nonlinear Dynamics and Control of Bi-stable Composites for Morphing Applications*, Ph.D. thesis, University of Bristol, 2009.
- [27] A. H. Nayfeh, D. T. Mook, *Nonlinear Oscillations*, John Wiley & Sons, 1979.

- [28] B. Balachandran, A. H. Nayfeh, Observations of modal interactions in resonantly forced beam-mass structures, *Nonlinear Dynamics* 2 (1991) 77–117.
- [29] K. D. Murphy, L. N. Virgin, S. A. Rizzi, Experimental snap-through boundaries for acoustically excited, thermally buckled plates, *Experimental Mechanics* 36 (1996) 312–317.
- [30] J. M. T. Thompson, H. B. Stewart, *Nonlinear Dynamics and Chaos*, John Wiley & Sons, 2002.
- [31] A. F. Arrieta, P. Hagedorn, A. Erturk, D. J. Inman, A piezoelectric bistable plate for nonlinear broadband energy harvesting, *Applied Physics Letters* 97 (2010) 104102.